Indian Journal of Chemistry
Vol. 56A, December 2017, pp. 1293-1301

Photocatalytic decolourisation of a toxic dye, Acid Blue 25, with graphene based N-doped titania

Susmita Sen Gupta* & Dhruba Chakrabortty
Department of Chemistry, B N College, Dhubri, Assam, India
Email: susmitasengupta21@gmail.com

Received 20 December 2016; revised and accepted 22 November 2017

This study investigates adsorption of Acid Blue 25 dye and photocatalytic decolourisation with graphene based nitrogen doped TiO_2. The prepared material has been characterised by XRD, BET, DRS, PL, TEM and XPS study. The photocatalytic reaction was carried out after the attainment of adsorption equilibrium between graphene based nitrogen doped TiO_2 and dye. The photocatalyst dose, initial dye concentration and solution pH are found to influence both the processes. The percentage decolourisation increases on increase of amount of catalyst from 95.57% (load: 0.125 g L^{-1}) to 99.91% (load: 0.75 g L^{-1}). However, further increase of the catalyst dose to 1.25 g L^{-1} leads to decrease in the extent of decolourisation. The decolourisation is favoured by lower dye concentration. The solution pH influences the reaction process and at pH 3.0, the material can decolourise almost 99% of the dye within 180 min of irradiation time. COD results reveal ~99% mineralisation of the dye on 420 min of irradiation. The percentage decolourisation of the dye is higher with graphene based nitrogen doped TiO_2 as compared to $NTiO_2$ or TiO_2 P25. The adsorption interaction follows the Lagergren first order model and modified Langmuir-Hinselwood model is preferably followed by dye decolourisation.

Keywords: Degradation, Dye degradation, Photocatalytic decolourisation, Graphene based N-TiO_2, Titania

Dye pollutants produced from the textile industries are a major source of environmental contamination. These effluents contain pollutants that exhibit toxic effects against microbial organisms and can be hazardous and carcinogenic to mammals[1.] One of the most important classes of commercial dyes is anthraquinonic dyes, mainly used for dyeing wool, polyamide and leather[2]. Acid Blue 25, an anthraquinoic dye, has wide application in wool, nylon, silk, paper, ink, aluminum, detergent, wood, fur, cosmetics, biological stain, etc.[3] This dye causes skin and eye irritation, and may also create respiratory problems. Thus, the decontamination of this dye is major concern to the environmentalists.

The use of semiconducting oxide materials as photocatalyst for organic pollutants, including dyes, provide a strong scientific incentive for ongoing research[4]. TiO_2 is one of the most widely used and investigated materials which has the advantages of being inexpensive, chemically stable, and nontoxic. However, because of the high intrinsic band gap (~3.0 eV), only ~ 4% of the incoming solar energy on the earth's surface can be utilized. Therefore, considerable efforts have been made to enhance the photosensitivity of TiO_2-based catalyst further into the visible-light region, using dopants[5]. Although various metals have been used for this purposes[6-9], the thermal instability and increase in carrier trapping, often lead to decrease the photocatalytic efficiency of metal-doped TiO_2[10]. To overcome these difficulties, anions are used as dopant for TiO_2[11-13]. Of the various anionic dopants, N-doping was found to be the most efficient[14-17]. The improvement of photocatalytic activity of N doped TiO_2 is mainly due to narrowing of the band gap by mixing of the N 2*p* states with O 2*p* states[18]. Moreover, the creation of N-induced midgap level[19] contributes to the enhancement of photocatalysis.

Graphene, an atomic sheet of sp^2-bonded C atoms arranged in a honeycomb structure[20], is an attractive material for preparing graphene containing inorganic composites due to its unique electronic property, high transparency, flexible structure and large specific surface area[21]. The graphene/inorganic composites possess the advantageous combination of excellent properties that are not found in the individual components. Incorporation of catalyst particle like TiO_2 onto an individual graphene or reduced graphene oxide (RGO) sheet with good distribution offers greater versatility in carrying out selective catalytic reactions[22]. The composite material has the advantages of retarding charge recombination and increasing reaction sites due to the high surface-to-volume ratio[23]. It has already been reported that N doping in TiO_2 decreases the band gap, facilitating the use of visible light. Thus, the graphene based N doped materials will provide an improved photocatalytic degradation of pollutants from water.

Keeping this in view, the present work aims to synthesis a graphene based N-doped photocatalyst for decontamination of Acid Blue 25 from aqueous system.

Materials and Methods

$TiCl_3$ (15%, Loba Chemie) and 25% NH_3 solution (EMerck) were used as sources of titanium and nitrogen, respectively. The graphite powder was procured from Sigma-Aldrich. TiO_2 P25 (AEROXIDE, Evonik (Degussa) Industries AG, Germany) was used as reference. Acid Blue 25 [1-amino-9,10-dihydro-9,10-dioxo-4-(phenylamino)-2-anthracenesulfonic acid, monosodium salt] (C.I. number: 62055, molecular formula: $C_{20}H_{13}N_2NaO_5S$) was procured from Sigma-Aldrich and used without further purification. All other reagents ($KMnO_4$, H_2SO_4, H_3PO_4, H_2O_2, HCl and ethanol) were of analytical grade.

Preparation of the catalysts, $NTiO_2$-RGO and TiO_2 P25-RGO

$NTiO_2$ was prepared by following the method published elsewhere[24]. In brief, 150 mL of $TiCl_3$ was taken in a Teflon beaker and 100 mL aqueous NH_3 solution was added drop-wise with constant stirring at 353 K over 3 hrs. The colour of the mixture first changed from deep purple to brownish black and then became brownish-yellow. The solid precipitate was separated and washed with distilled water several times and finally dried in air oven at 343 K. The sample was then calcined at 623 K for 4 h in a muffle furnace to get a yellowish brown powder.

An improved Hummers' method was used for the synthesis of graphene oxide[25, 26]. Graphite powder (1.5 g) and $KMnO_4$ (9.0 g) were consecutively added into a 9:1 mixture of concentrated H_2SO_4/H_3PO_4 (180:20 mL) under continuous stirring. The reaction was heated at 323 K and stirred for 12 h. Then the reaction was cooled to room temperature and poured into ice with 30% H_2O_2 (3 mL). The mixture was then centrifuged and washed with water, 30% HCl solution and ethanol. The solid product thus obtained (GO) was finally dried at 353 K.

The synthesis of $NTiO_2$-RGO composite was obtained via a hydrothermal method as described by Zhang *et al.*[27] Briefly, 0.2 g of GO was dissolved in a mixture of 20 mL H_2O and 10 mL ethanol by ultrasonic treatment for 1 h, and 0.2 g of $NTiO_2$ was added to the obtained GO solution and stirred for another 2 h to get a homogeneous suspension. The suspension was then placed in a Teflon-sealed autoclave and maintained at 393 K for 3 h to simultaneously achieve the reduction of GO and the deposition of $NTiO_2$ on the carbon substrate. Finally, the resulting composite was recovered by filtration, washed with water several times, and dried at room temperature.

TiO_2 P25-RGO was synthesised in a similar way, using TiO_2P25 instead of $NTiO_2$.

Characterisation

The samples were characterised by recording the XRD patterns (Rigaku Miniflex diffractometer using nickle-filtered Cu-K_α radiation), XPS spectra (Kratos AXIS Ultra DLD XPS system equipped with a monochromatic Al-Kα source), diffuse reflectance spectra (HITACHI-400 spectrophotometer), HR-TEM images (JEOL JEM 2100) and photoluminescence (HitachiF-2500 FL spectrophotometer). The BET surface area of the catalyst was measured by nitrogen adsorption method at 77 K with the help of Quantachrome Autosorb-1C surface area analyser, using BET equation.

Adsorption studies

A pre-weighed sample of the adsorbent material and a measured volume of dye solution were taken in a 100 mL Erlenmeyer flask, and the mixture was agitated in a thermostatic water bath shaker (NSW, Mumbai, India) for a fixed time interval under dark. The mixture was centrifuged (Remi R 24), and the dye solution remaining unadsorbed in the supernatant liquid was determined at λ_{max} = 502 nm (Elico SL 177, India). Various experimental parameters, viz., influence of adsorbent load (0.125–1.25 g L^{-1}), initial dye concentration (18.0–36.0 µmol L^{-1}) and pH (3.0–11.0) on dye adsorption were studied.

Photocatalytic activity

Details of the catalytic experiment with the schematic diagram of the reactor is given elsewhere.[28] In brief, a glass reactor with water circulation facility was used for catalytic reaction of dye. The reactor comprised a 250 W halogen bulb (as the source of visible light) fitted with a glass filter to cut-off short wavelengths ($\lambda < 420$ nm).

In a typical reaction, a fixed volume of dye solution and requisite amount of catalyst were taken in the reactor and kept in dark for 60 min under stirring to attain the adsorption–desorption equilibrium. The mixture was then exposed to visible light under constant stirring with the help of a magnetic stirrer. The concentration of dye after adsorption (60 min) was considered as the initial concentration for photocatalytic study. The reacting dye solution was collected at regular intervals and concentration of the dye was measured with the help of a visible spectrometer as mentioned before. The extent of dye decolourisation on varying catalyst load (0.125–1.25 g L^{-1}), initial dye concentration (18.0–36.0 µmol L^{-1}) and pH (3.0–11.0) was studied.

Mineralisation of dye

Chemical oxygen demand (COD) is an index of water pollution by organics and it is a parameter used for quality discharge. COD is the measure of oxygen equivalent of the organic content in an organic sample, which is susceptible to oxidation by a strong oxidant. The dichromate reflux method was adapted to estimate COD[29] given by,

$$\text{Mineralization (\%)} = \{(COD_0 - COD_t) \times 100\} / COD_0$$

where COD_0 = COD of original dye, COD_t = COD of degraded dye after time '*t*' (hour)

Result and Discussion

Characterization of photocatalyst

Figure 1 shows the XRD pattern of $NTiO_2$-RGO along with GO, $NTiO_2$ and TiO_2 P25-RGO. The pattern of $NTiO_2$ and $NTiO_2$-RGO confirmed the formation of pure anatase phase of TiO_2. Like TiO_2 P25, the TiO_2P25-RGO contained both anatase and rutile phase as is evident from the XRD pattern. The XRD pattern of GO showed characteristic peak for the (001) plane. The absence of GO(001) peak in $NTiO_2$-RGO and TiO_2P25-RGO may be ascribed to the fact that GO was reduced to graphene during the hydrothermal reaction.

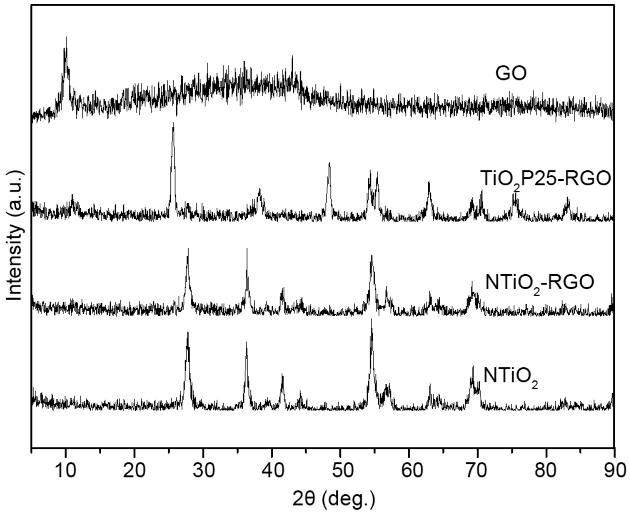

Fig. 1 — XRD of GO, TiO_2P25-RGO, $NTiO_2$ and $NTiO_2$-RGO.

The particle size of $NTiO_2$, TiO_2P25-RGO and $NTiO_2$-RGO are calculated from (101) peak using Scherrer equation,[10,30]

$$D = \frac{\kappa \lambda}{\beta \, Cos\theta}$$

where, κ = 0.9, $\lambda = 0.154$ nm, β = full width half maxima and θ = defraction angle. The particle size of $NTiO_2$, $NTiO_2$-RGO and TiO_2P25-RGO was calculated as 6.2 nm, 26.01 nm and 20.77 nm, respectively.

The BET surface areas and pore volumes of $NTiO_2$-RGO, $NTiO_2$, TiO_2P25-RGO and GO are given in Table S1 (Supplementary Data). Amongst these, $NTiO_2$-RGO possesses the highest BET surface area (229.72 m^2 g^{-1}).

The band gap energies of $NTiO_2$ and $NTiO_2$-RGO were determined using UV-visible diffused reflectance spectroscopy (Fig. 2). Wider visible light adsorption is observed in the case of $NTiO_2$-RGO as compared to $NTiO_2$. The band gap energy, Eg, was calculated using the equation[31] Eg = 1420/λ, where λ is the wavelength (nm) corresponding to the point of intersection between the vertical and horizontal line in the spectra. The band gap energy in $NTiO_2$ and $NTiO_2$-RGO was found to be 2.94 eV and 2.38 eV

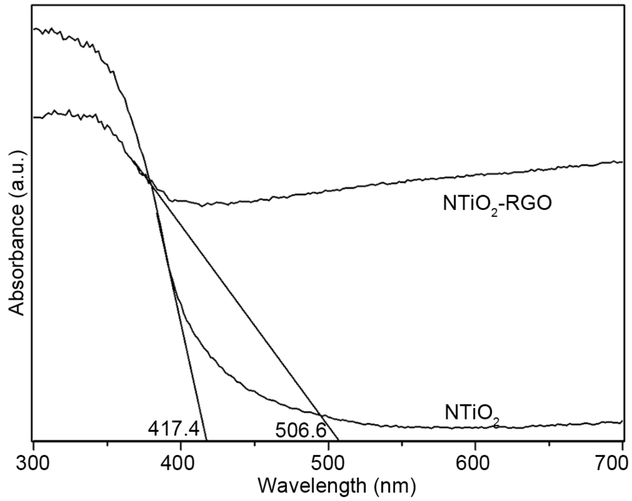

Fig. 2 — Diffuse reflectance spectra of $NTiO_2$ and $NTiO_2$-RGO.

respectively, indicating a red shift due to the presence of graphene matrix. The extending of visible light absorption is likely to be one of the reasons for higher photocatalytic activity of $NTiO_2$-RGO as compared to $NTiO_2$.

The N 1*s* XPS peak at 396 eV was assigned to β-N by Saha *et al.*[32] In our sample (Fig. 3) we observed the N 1*s* XPS peak near 396 eV (at 395.6 eV to be precise). This peak has been assigned to β-N forming Ti-N linkage. Since XRD does not indicate formation of TiN, this XPS peak may be due to β-N that substiutionally replaced O, forming the O-Ti-N bond.

Asahi *et al.*[18] reported that N 1*s* XPS peak at 396 eV is responsible for enhanced photocatalytic activity of N doped TiO_2. A linear increase in visible light response to the XPS intensity of the N at 396 eV was reported for N-doped TiO_2 by Irie *et al.*[33] According to Asahi *et al.*[18], the sites for photoactivity under visible light irradiation were those where N substitutionally replaced O, i.e., is the sites with atomic β-N which shows N 1*s* XPS peak at 396 eV. One of the reasons for the enhanced photoactivity in our catalyst may be due to the β-N present in the sample which shows XPS peak at 395.6 eV.

It is known that the efficiency of a photocatalyst depends on effective reduction of bulk/surface charge recombination. Graphene as electron transporting bridge and electron sink prevents the bulk/surface charge recombination by efficient charge separation and fast charge transportation. As photoluminous emission is due to the recombination of excited electrons and holes under light irradiation, the higher PL intensity shows the separation and combination of more photoinduced electron and holes inside the materials. If the photo-generated electrons and holes are transferred to other matters, i.e., quenching takes place, PL intensity will decrease.

In the present study (Fig. 4) the excitation wavelength for $NTiO_2$ is 421 nm while that for $NTiO_2$-RGO it is 510 nm. A hump has been observed in $NTiO_2$ around 470 nm which may be due to photoluminous emission arising from recombination of the excited electrons and holes. Absence of any such phenomenon indicates effective quenching due to the presence of graphene. Similar result was observed by Pei *et al.*[34] in their study of enhancement of photocatalytic efficiency for hydrogen evaluation by nanocomposite of N-doped TiO_2 with graphene oxide

The photocatalytic activity of a material is often influenced by the morphology of that material to a great extent. Graphene nanosheets have a tendency to congregate together to form multilayer agglomerates. The TEM image (Fig. 5) shows the crystalline nature of the graphene nanosheet which was prevented from re-aggregation by direct interaction between N-TiO_2 and graphene nanosheets. The plate-like texture of monolayer GO with a large specific surface area possibly provided much more active sites than N-TiO_2 for photocatalytic reaction of dye. Similar observation was reported earlier.[34]

Adsorption studies

The adsorption experiments were carried out with dye concentrations in the range of 18 - 36 µmol L^{-1} with a constant $NTiO_2$-RGO amount of 0.25 g L^{-1} (pH 6.5 at 303 K). The extent of dye adsorption (%) decreased from 10.57% to 9.14% at equilibrium time of 60 min by increasing the Acid Blue 25

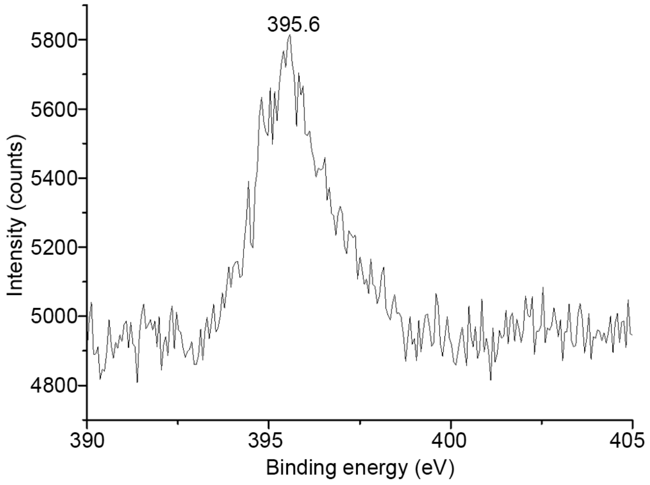

Fig. 3 — XPS of $NTiO_2$-RGO.

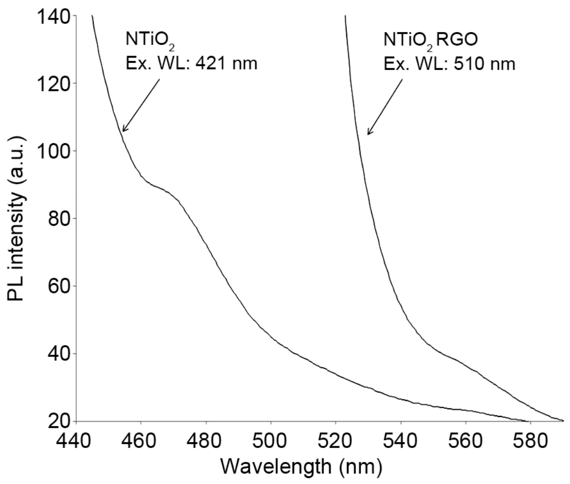

Fig. 4 — PL of $NTiO_2$ and $NTiO_2$-RGO.

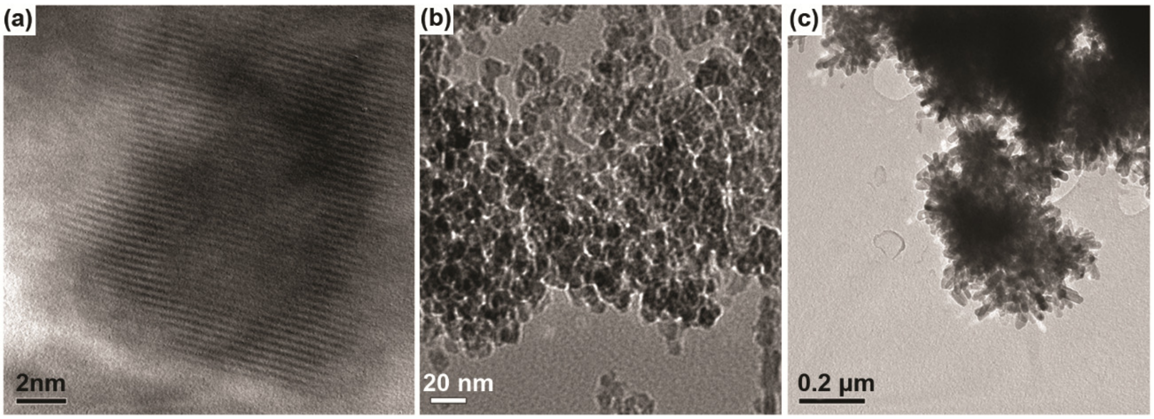

Fig. 5 — TEM of (a) GO, (b) $NTiO_2$ and (c) $NTiO_2$-RGO.

concentration (from 18.0 to 36.0 μmol L^{-1}) (Supplementary Data, Table S2). At low initial adsorbate concentration, the ratio of the number of dye species to the number of available adsorption sites was small and consequently the uptake was independent of the initial concentration. The dye species were driven to the adsorbent surface by the force generated due to the concentration gradient between the $NTiO_2$-RGO surface and the bulk solution. Under the same conditions, when the concentration of the dye was high, the active sites on $NTiO_2$-RGO would be surrounded by more dye molecules, and the active sites are likely to be saturated with dye cations[35].

With initial Acid Blue 25 concentration of 18.0 μmol L^{-1}, the uptake increased from 7.91% to 12.24% for $NTiO_2$-RGO dose of 0.125 to 0.75 g L^{-1}. The higher amount of adsorbent provided more surfaces for the dye to get adsorbed on. Moreover, the further increase of adsorbent dose (1.25 g L^{-1}) decreased the percentage adsorption to 11.81% (Supplementary Data, Table S2), which may be due to particle agglomeration[36].

The adsorbent-adsorbate interaction is often influenced by pH of the reaction medium. At equilibrium time of 60 min, the extent of adsorption was maximum (18.31%) at pH 3.0 and showed a steady decrease up to pH 11.0 (4.12%) ($NTiO_2$-RGO: 0.25 g L^{-1}, initial dye conc.: 18 μmol L^{-1}). A significantly high electrostatic attraction between the positively charged surface of the adsorbent and the anionic dye may favour the adsorption process at low pH. However, at high pH, the highly mobile OH^- ions will be preferred by the negatively charged adsorption sites on the adsorbent surfaces in comparison to the bulky dye anions[36].

In the case of $NTiO_2$, almost similar trends were observed in all the experimental variables. The adsorption increased from 7.0% to 10.29% for $NTiO_2$ dose of 0.125–0.75 g L^{-1} and then decreased to 7.60% (1.25 g L^{-1}) at 60 min. A maximum dye adsorption of 16.30% was observed at pH 3.0, which showed a steady decrease with 4.0 at pH 9.0 and so on.

The Langmuir isotherm[37] model was used to study the adsorption capacities of the dye on $NTiO_2$ and $NTiO_2$-RGO. The linear equation of the model is given by, $C_e/q_e = (1/bq_m) + (1/q_m)\ C_e$, where C_e = concentration of dye and at equilibrium, q_e = amount of dye adsorbed per unit mass of adsorbent and q_m = Langmuir monolayer adsorption capacity.

The q_m values calculated from the slope of the plots C_e/q_e versus C_e for $NTiO_2$-RGO and $NTiO_2$ were 2.69×10^{-3} mg g^{-1} and 1.30×10^{-3} mg g^{-1}, respectively. These results indicate that $NTiO_2$-RGO was a better adsorbent for dye as compared to $NTiO_2$.

Lagergren pseudo first-order model[38] was used to study the kinetics of adsorption interaction. The linear form of the equation is given by, $\log (q_e - q_t) = \log q_e - k_1 t$, where, q_e = amounts adsorbed per unit mass at equilibrium, q_t = amounts adsorbed per unit mass at any time t and k_1 = the first order rate constant. The $\log (q_e-q_t)$ versus t plots are linear (r = - 0.91 to - 0.99) for all the experimental variables.

The first order rate constants were influenced by the experimental variables. The k_1 values increased from 6.14×10^{-2} to 11.44×10^{-2} min^{-1} for the variation of adsorbent load of 0.125–0.75 g L^{-1} and decreased to 10.31×10^{-2} min^{-1} (at 1.25 g L^{-1}). Similar trends were observed for other cases also (Supplementary Data, Table S3).

In the case of $NTiO_2$, almost similar trends were noticed, e.g., the k_1 values were in the range of 6.60×10^{-2} to 3.33×10^{-2} min^{-1} for the variation of solution pH 3.0 to 9.0.

The optimum conditions for maximum adsorption are summarized as follows: adsorbent load: 0.25 g L^{-1}, dye conc.: 18–36 μmol L^{-1}, pH: 6.5, and temp: 303 K.

Photocatalytic studies

The influence of $NTiO_2$-RGO load on decolourisation of Acid Blue 25 was studied for the variation of catalyst amount (0.125 to 1.25 g L^{-1}, Supplementary data, Fig S1 (a). At equilibrium (180 min), decolourisation of dye (initial dye conc.: 18 μmol L^{-1}) increased from 95.57% (load: 0.125 g L^{-1}) to 99.91% (load: 0.75 g L^{-1}). The larger amount of photocatalyst provided higher number of photo-electrons that enhanced the decolourisation process.[39] On the other hand, further rise in catalyst load (1.25 g L^{-1}) decreased the decolourisation to 99.45%. The excess catalyst load may hinder the incident light, which may decrease the concentration of $^{\cdot}OH$ radicals, a primary oxidant in the photocatalytic system[40], resulting in lowering of the dye decolourisation process.

In the case of $NTiO_2$, an almost similar trend was observed.[24] However, in all the cases, decolourisation efficiency was better for $NTiO_2$-RGO as compared to $NTiO_2$; 0.25 g L^{-1} of $NTiO_2$-RGO decolourised ~98.13% of Acid Blue 25, whereas the same amount of $NTiO_2$ could decolourise only 77% of the dye (Supplementary Data, Fig. S2) Thus, the introduction of graphene to $NTiO_2$ boosted the dye decolourisation process.

The degradation profile of Acid Blue 25 with catalyst load 0.25 g L^{-1} under varying concentration of dye was studied. The decolourisation by $NTiO_2$-RGO decreased from 98.13% to 79.09% on increasing the dye concentration from 18.0 to 36.0 μmol L^{-1} (Supplementary Data, Fig. S1(b)). Similarly, in the case of $NTiO_2$ the decolourisation decreased from 88.8% to 67.8% for same range of dye concentration (Supplementary Data, Fig. S3).

At higher concentration, the active sites of catalyst were covered by a larger number of dye molecules, obstructing the production of $^{\bullet}OH$ radicals on the surface. This may decrease the decolourisation process, as fewer number of $^{\bullet}OH$ radicals were available to oxidize large number of dye molecules.[41] Moreover, a large number of dye molecules had to react with the same amount of $^{\bullet}OH$ radical, leading to a decrease in the decolourization efficiency.[42]

The decolourisation of dye was favoured at lower pH and a gradual decrease in percentage decolourisation was noticed as the solution pH increases. Thus, at pH 3.0, 0.25 g L^{-1} $NTiO_2$-RGO decolourised ~100% Acid Blue 25 within 60 min (Supplementary Data, Fig. S1(c)). On the other hand, only ~ 42% dye decolourisation occurred at pH 11.0 (at 240 min). An almost similar trend was noticed in the case of $NTiO_2$ (at pH 3.0: 99.4%, at pH 11.0: 35.8%) (Supplementary Data, Fig. S4).

The solution pH is an important parameter in the photodegradation process as the production of hydroxyl radicals is influenced by the solution pH. The $^{\bullet}OH$ radicals were formed by the reaction between OH^- ions and positive holes. At low pH, positive holes acted as the major oxidation species, and at neutral or higher pH, $^{\bullet}OH$ radicals were considered as predominant species. In alkaline medium the coulombic repulsion between the negatively charged surface of $NTiO_2$-RGO or $NTiO_2$ and the OH^- ions hinders the formation of $^{\bullet}OH$ and thus decreases the photoxidation and decolourisation[43]. Moreover, the presence of sulphonate group in Acid Blue 25 favoured its adsorption at low pH, which definitely helped the decolourisation process.

The modified Langmuir-Hinselwood (L-H) mechanism was applied to study the kinetics of Acid Blue 25 decolorisation. At sufficient low concentration of dye, the L-H relation can be expressed as, $\ln(C_0/C) = kK_et = k't$, where, C = concentration of dye, C_0= initial concentration of dye, k (min^{-1}) = apparent reaction rate constant, K_e = apparent equilibrium constant for the adsorption of the dye on the catalyst surface and k' (min^{-1}) is the overall rate constant.

By plotting $\ln(C_0/C)$ as a function of irradiation time through regression, the k' (min^{-1}) constant for each catalyst sample can be obtained from the slopes.

The overall rate constant for dye decolourisation reactions was studied under different experimental parameters, namely, change of catalyst load, initial dye concentration and solution pH. Although the curves did not pass through the origin as required by the model, the intercepts were close to zero (varied from -0.208 to + 2.115) (Supplementary Data, Fig. S5).

The Langmuir-Hinshelwood rate constants of dye decolourisation by $NTiO_2$-RGO showed a steady increase from 17.8×10^{-3} min^{-1} (catalyst load: 0.125 g L^{-1})

to 41.2×10^{-3} min^{-1} (catalyst load: 0.75 g L^{-1}) and then decreased (31.0×10^{-3} min^{-1}) for catalyst load of 1.25 g L^{-1}. An increase in initial dye concentration from 18.0 µmol L^{-1} to 36.0 µmol L^{-1}decreased the rate constant from 17.8×10^{-3} min^{-1} to 8.70×10^{-3} min^{-1}. In terms of solution pH, the rate of decolourisation favoured lower pH (34.6×10^{-3} min^{-1} at pH 3.0 to 3.4×10^{-3} min^{-1} at pH 11.0) (Supplementary Data, Table S3). These results are consistent with the influence of experimental parameters on photocatalytic decolourisation.

Almost similar trends were observed for $NTiO_2$ as catalyst. The rate constant showed a steady decreased from 12.6×10^{-3} min^{-1} to 6.2×10^{-3} min^{-1} by increasing the dye concentration from 180 µmol L^{-1} to 36.0 µmol L^{-1}. In all the cases, the dye–$NTiO_2$-RGO interactions yielded larger first order rate constant values as compared to dye–$NTiO_2$ interactions.

Decolourisation of Acid Blue 25 on $NTiO_2$-RGO with TiO_2 P25 and TiO_2 P25-RGO

In a blank experiment (carried out with 18.0 µmol L^{-1} dye for 180 min in absence of catalyst under visible light), only 2.2% decolourisation was observed (Fig. 6). A comparative study was carried for the decolourisation of Acid Blue 25 by TiO_2 P25 and TiO_2 P25-RGO. It was observed that from an initial dye concentration of 18.0 µmol L^{-1} (irradiation time 180 min), 0.25 g L^{-1} TiO_2 P25 could decolourised ~9.0% of dye, while ~31.0% decolourisation was observed with TiO_2 P25-RGO. It has already been mentioned that 0.25 g L^{-1} of $NTiO_2$ decolourised ~77.0% of Acid Blue 25. The study revealed that $NTiO_2$-RGO decolourised the dye more efficiently than TiO_2 P25, TiO_2 P25-RGO and $NTiO_2$.

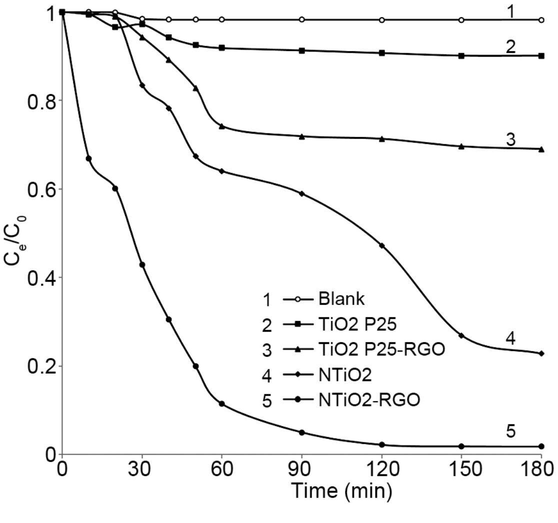

Fig. 6 — Comparison of the photocatalytic degradation of Acid Blue 25 by TiO_2 P25 (curve 2), TiO_2P25-RGO, (curve 3) $NTiO_2$ (curve 4) and $NTiO_2$-RGO (curve 5). [(Initial dye conc.: 18.0 µmol L^{-1}, catalyst load: 0.25 g L^{-1}, Temp.: 303 K].

The Langmuir-Hinselwood rate constant of Acid Blue 25 decolourisation by $NTiO_2$-RGO was higher as compared to the rate constants of the dye decolourisation by TiO_2 P25 (~ 40%), TiO_2P25-RGO (~10%) and even than $NTiO_2$ (~3%) under similar experimental conditions (k' for TiO_2P25: 6.0×10^{-4} min^{-1}, TiO_2P25-RGO: 2.3×10^{-3} min^{-1}, N-TiO_2: 8.6×10^{-3} min^{-1}).

Mechanism of dye degradation

The doping of a foreign element (e.g., N, C, F etc) in metal oxide, like TiO_2 may create oxygen vacancies. Such oxygen vacancies in TiO_2 can lead to an enhancement of photocatalytic activity as mentioned by Asahi *et al.*[18] The high charge recombination rate in $NTiO_2$ restricts the photogenerated charges in separation and transportation on to the catalyst surface. Thus, $^{\bullet}OH$ radicals and O_2 intermediate species are created by reacting with absorbed H_2O molecules for the photodecomposition of dye[23]. On the other hand, the electron acceptor character and high electronic conductivity of graphene in $NTiO_2$-RGO allows the photo-generated charges to be separated efficiently and transported to the graphene layer for radical generation[44]. Besides, the strong π-π stacking interaction between aromatic regions of graphene and dye molecules may create a high affinity of the dye towards the catalyst. Similar observation was reported earlier[45].

Thus, the synergic incorporation of nanometer-sized $NTiO_2$ and excellent charge transport behaviour of graphene sheets improved photoelectrochemical properties of $NTiO_2$-RGO compared to the TiO_2P25 or $NTiO_2$[45].

Mineralization of dye

The extent of degradation/mineralization of an organic species is often understood by the change in chemical oxygen demand (COD). With initial dye concentration of 18.0 µmol L^{-1} and $NTiO_2$-RGO load 0.25 g L^{-1}, a steady decrease in COD with the increase in the irradiation time was observed. The percentage mineralisation of the dye increased from 14.5% to 98.0% as the photocatalytic reaction was carried out from 1 h to 7 h. Moreover, the percentage mineralization was less compared to percentage decolourisation at a particular time. Thus, after 3 h of

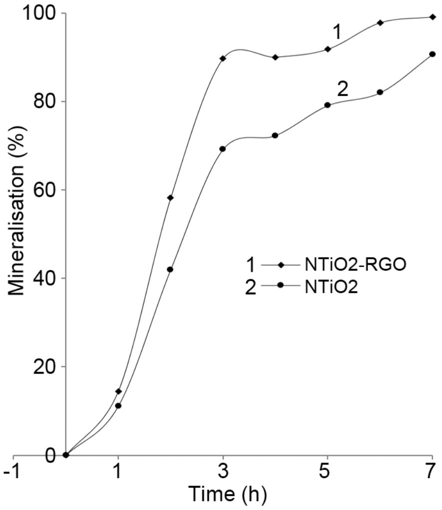

Fig. 7 — Comparison of % mineralization of Acid blue 25 on $NTiO_2$-RGO (curve 1) and $NTiO_2$ (curve 2) at different time intervals.

reaction, the percentage mineralization was ~90%, while the percentage decolourisation reached almost 99%. Similar trend was observed in the case of $NTiO_2$. The mineralisation increased from 11% to 90% as the reaction time increased from 1 h to 7 h. In this case also, the percentage mineralisation was less (69.2% at 3 h) as compared to percentage decolourisation (88.8% at 3 h) (Fig. 7).

During the decolourisation process, some smaller uncoloured products might be produced which were responsible for comparatively higher values of COD. However, being uncoloured, these products were responsible for higher decolourisation values.

Conclusions

The photocatalytic decolourisation of Acid Blue 25 was studied using graphene based N-doped TiO_2 and its efficiency was compared with that of $NTiO_2$. The experimental variables ($NTiO_2$-RGO/$NTiO_2$ dose, initial dye concentration and solution pH) influenced the adsorption and dye decolourisation process. A higher catalyst load had a positive influence on dye decolourisation, however above the catalyst load of 1.25 g L^{-1}, there was a decrease in the efficiency. The decrease in initial dye concentration enhanced the decolourisation process. Moreover, the acidic pH favoured the decolourisation of dye compared to neutral and alkaline pH. Adsorption interactions followed Lagergren first-order kinetic model, whereas the photo-catalytic decolourisation of dye fitted the modified Langmuir–Hinshelwood model. Parameters, such as $NTiO_2$-RGO/$NTiO_2$ dose, initial dye concentration and solution pH played an important role affecting the reaction rate constants for both the processes, i.e. adsorption as well as decolourisation. The percentage mineralisation of the dye was found to be 11.1% in 1 h, which went up to 90.7% in 7 h.

Supplementary Data

Supplementary Data associated with this article are available in the electronic form at http://www.niscair.res.in/jinfo/ijca/IJCA_56A(12)1293-1301_SupplData.pdf.

Acknowledgement

The authors are thankful to Dr. Shuguo Ma of College of Engineering and Computing, University of South Carolina, USA, for XPS measurements. We are thankful to IIT-Guwahati, India for HR-TEM measurement.

References

1 Marçal L, de Faria E H, Saltarelli M, Calefi P S, Nassar E J, Ciuffi K J, Trujillano R, Vicente M A, Korili S A & Gil A, *Ind Eng Chem Res,* 50 (2011) 239.
2 Bouzaida I, Ferronato C, Chovelon J M, Rammah M E & Herrmann J M, *J Photochem Photobiol A: Chem,* 168 (2004) 23.
3 Ghodbane H & Hamdaoui O, *Chem Eng J,* 160 (2010) 226.
4 Serpone N & Pilezzetti E (Eds.) *Photocatalysis: Fundamentals and Applications*, (Wiley-Interscience, New York) 1989.
5 Diwald O, Thompson T L, Zubkov T, Goralski E G, Walck S D & Yates J T Jr, *J Phy Chem B,* 108 (2004) 6004.
6 Arabatzis I M, Stergiopoulos T, Bernard M C, Labou D, Neophytides S G & Falaras P, *Appl Catal B: Environ,* 42 (2003) 187.
7 Zhao D, Chen C, Wang Y, Ma W, Zhao J, Rajh T & Zang L, *Environ Sci Technol,* 42 (2008) 308.
8 Kowalska E, Remita H, Colbeau-Justin C, Hupka J & Belloni J, *J Phy Chem C,* 112 (2008) 1124.
9 Hao H & Zhang J, *Microporous Mesoporous Mater,* 121 (2009) 52.
10 Cong Y, Zhang J, Chen F & Anpo M, *J Phys Chem C,* 111 (2007) 6976.
11 Liu G, Chen Z, Dong C, Zhao Y, Li F, Lu G Q & Cheng H-M, *J Phys Chem B,* 110 (2006) 20823.
12 Bidaye P P, Khushalani D & Fernandes J B, *Catal Lett,* 134 (2009) 169.
13 Rengifo-Herrera J A, Pierzchała K, Sienkiewicz A, Forró L, Kiwi J, Moser J E & Pulgarin C, *J Phys Chem C,* 114 (2010) 2717.
14 Zhao Y, Qiu X & Burda C, *Chem Mater,* 20 (2008) 2629.
15 Li G, Yua J C, Zhanga D, Hua X & Lau W M, *Sep Purif Technol,* 67 (2009) 152.
16 Dong F, Wang H, Wu Z & Qiu J, *J Colloid Interf Sci,* 343 (2010) 200.
17 Collazzo G C, Foletto E L, Jahn S L & Villetti M A, *J Environ Manag,* 98 (2012) 107.
18 Asahi R, Morikawa T, Ohwaki T, Aoki K & Taga Y, *Science,* 293 (2001) 269.

19 Nakamura R, Tanaka T & Nakato Y, *J Phys Chem B,* 108 (2004) 10617.

20 Geim A K & Novoselov K S, *Natural Mater,* 6 (2007) 183.

21 Chen C, Cai W, Long M, Zhou B, Wu Y, Wu D & Feng Y, *ACS Nano,* 4 (2010) 6425.

22 Kamat P V, *J Phy Chem Let,* 1 (2010) 520.

23 Lee E, Hong J-Y, Kang H & Jang H, *J Hazard Mater,* 219–220 (2012) 13.

24 Chakrabortty D & Sen Gupta S, *J Environ Sci,* 25 (2013) 1034.

25 Marcano D C, Kosynkin D V, Berlin J M, Sinitskii A, Sun Z Z, Slesarev A, Alemany L, Lu W & Tour J M, *ACS Nano,* 4 (2010) 4806.

26 Li B, Liu T, Wang Y & Wang Z, *J Colloid Interf Sci,* 377 (2012) 114.

27 Zhang H, Lv X, Li Y, Wang Y& Li J, *ACS Nano,* 4 (2010) 380.

28 Chakrabortty D & Sen Gupta S, *Desalination Water Treat,* 52 (2014) 5528.

29 APHA, Standard Methods for the Examination of Water and Wastewater. American Public Health Association, 19th Edn, Washington, DC, USA, 1999.

30 Lin J, Lin Y, Liu P, Meziani M J, Allard L F & Sun Y P, *J Am Chem Soc,* 124 (2002) 11514.

31 Shao G-S, Zhang X-J & Yuan Z-Y, *Appl Catal B: Environ,* 82 (2008) 208.

32 Saha N C & Tomkins H C J, *J Appl Phy,* 72 (1992) 3072.

33 Irie H, Watanabe Y & Hashimoto K, *J Phy Chem B,* 107 (2003) 5483.

34 Pei F, Liu Y, Xu S, Lu J, Wang C & Cao S, *Int J Hydrogen Energy,* 38 (2013) 2670.

35 Bhattacharyya K G, Sen Gupta S & Sarma G K, Kinetics, *Desalination Water Treat,* 53 (2015) 530.

36 Simakov SA & Tsur Y, *J Nanopart Res,* 9 (2007) 403.

37 Langmuir I, *J Am Chem Soc,* 40 (1918) 1361.

38 Lagergren S, *Kungliga Svenska Vetenskapsakademiens, Handlingar*, 24 (1898) 1.

39 Bizani E, Fytianos K, Poulios I & Tsiridis V, *J Hazard Mater,* 136 (2006) 85.

40 Sun J H, Qiao L P, Sun S P & Wang G L, *J Hazard Mater,* 155 (2008) 312.

41 Grzechulska J & Morawski A W, *Appl Catal B,* 36 (2002) 45.

42 Daud N K, Akpan U G & Hameed B H, *Desalination Water Treat,* 37 (2012) 1.

43 Sleiman M, Vildozo D, Ferronato C & Chovelon J M, *Appl Catal B: Environ,* 77 (2007) 1.

44 Wang X, Zhi L & Mullen K, *Nano Lett,* 8 (2008) 323.

45 Liu Z, Robinson J T, Sun X & Dai H, *J Am Chem Soc,* 130 (2008) 10876.